



Article

Photoacoustic Effect of Near-Infrared Absorbing Organic Molecules via Click Chemistry

Wenqing Zhu ¹, Zongcheng Miao ^{1,*}, Yaqin Chu ¹, Liaoliao Li ², Lei Wang ^{3,*} and Dong Wang ^{2,*}

¹ School of Chemical and Environmental Engineering, Anhui Polytechnic University, Wuhu 241000, China; zwq_1021@163.com (W.Z.); yaqinjudinda@163.com (Y.C.)

² School of Materials Science and Engineering, University of Science and Technology Beijing, Beijing 100083, China; ll285687@163.com

³ Key Laboratory of Auxiliary Chemistry and Technology for Chemical Industry, Ministry of Education, Shaanxi University of Science and Technology, Xi'an 710021, China

* Correspondence: miaozongcheng@ahpu.edu.cn (Z.M.); wanglei@sust.edu.cn (L.W.); wangdong@ustb.edu.cn (D.W.); Tel.: +86-189-9115-0632 (Z.M.)

Abstract: Near-infrared dyes were developed to be contrast agents due to their ability to improve the productivity of photoacoustic (PA) imaging and photothermal therapy (PTT) treatments. During the article, we described in detail the PA and PT effects of a category of organic molecules. F₄-TCNQ could potentially cause a red-shift in the peak PA intensity. The results show that the PTT intensity of the near-infrared dyes with phenyl groups were higher than near-infrared dyes with thiophene groups. We also investigated the photodynamic treatment effect of C1b to demonstrate that these dyes are highly desirable in biochemistry. The high photoacoustic intensity of the organic molecules and the good yield of reactive oxygen species could indicate that these dyes have good potential for a wide range of imaging applications. Finally, we embedded the dye (C1b) in a liposomal hydrophobic phospholipid bilayer (C1b⊂L) to facilitate the application of hydrophobic dyes in biomedical applications, which can be absorbed by cells with good compatible and high stability for the imaging of cellular PA.

Keywords: near-infrared; photoacoustic imaging; photothermal treatment; photodynamic therapy



Citation: Zhu, W.; Miao, Z.; Chu, Y.; Li, L.; Wang, L.; Wang, D.

Photoacoustic Effect of Near-Infrared Absorbing Organic Molecules via Click Chemistry. *Molecules* **2022**, *27*, 2329. <https://doi.org/10.3390/molecules27072329>

Academic Editors: Angelo Sampaolo and Hongpeng Wu

Received: 27 February 2022

Accepted: 31 March 2022

Published: 4 April 2022

Publisher's Note: MDPI stays neutral with regard to jurisdictional claims in published maps and institutional affiliations.



Copyright: © 2022 by the authors. Licensee MDPI, Basel, Switzerland. This article is an open access article distributed under the terms and conditions of the Creative Commons Attribution (CC BY) license (<https://creativecommons.org/licenses/by/4.0/>).

1. Introduction

Photoacoustic (PA) imaging has been developed as a noninvasive real-time modality to be used for biomedical imaging, with promising applications in terms of increased penetration depth and superior spatial resolution in comparison to conventional optical imaging techniques. PA imaging can effectively image the structure and function of biological tissues. PA imaging contrast agents enhance image contrast and resolution by modifying the optical and acoustic properties of local tissues, thereby significantly improving image output [1–4]. Near-infrared light-absorbing materials have acquired favor as investigational PA contrast agents. There are two reasons for this: on the one hand, native light from tissues has the lowest absorption in the near-infrared (NIR) region, and on the other hand, PA contrast agents can potentially be used in photothermal therapy (PTT) while the materials show a strong Near-infrared absorption [5]. PA imaging contrast agents with near-infrared (NIR) window absorption and high PA intensity can effectively enhance the use of PA imaging in biomedical applications. Several NIR absorbing contrast agents were reported for photoacoustic imaging and photothermal therapy treatment, for example, near-infrared dyes [6], gold-based nanoparticles [7–9], along with other inorganic materials [10,11]. Nevertheless, NIR absorbing low molecular weight organic dyes exhibit excellent biodegradability and potentially short-term toxicity compared to other inorganic contrast agents which are better suited for photoacoustic and photothermal contrast agents [12].

Some organic dyes have the maximal absorption in the near infrared range and are extensively applied as PA contrast agents. For example, cyanide [13], porphyrins [14] and boron dibromothiophene derivatives [3]. The discovery of new photoacoustic molecular materials has been restricted by the paucity of systematic studies on factors affecting PA effects, which has led to poor guidance in the study of molecular photoacoustic contrast agent design [4,15,16]. Lately, the chemistry of [2 + 2] cycloaddition-cycloreversion reactions between tetracyanoethylene (TCNE), 7,7,8,8-tetracyanodimethane (TCNQ) or 2,3,5,6-tetrafluoro-7,7,8,8-tetracyanodimethane (F₄-TCNQ) and ‘electronically chaotic’ alkynes were focused on [17–39]. The consequent adducts, specifically those composed of F₄-TCNQ formation, had excellent solubility and could be easily produced in high yields. It is worth noting that these adducts display intense absorption in an area of 700–900 nm that makes them very applicable as contrast agents for PAI.

The purpose of our study was to investigate the PA and PTT effectiveness of organic molecules with the clicked 7,7,8,8-tetracyanoquiodimethane (TCNQ) and 2,3,5,6-tetrafluoro-7,7,8,8-tetracyanoquiodimethane (F₄-TCNQ) as well as modifying all kinds of functional groups in various locations. The organic molecule clicked by F₄-TCNQ can cause a significant red shift of the PA intensity peak compared to four different molecules. In addition, the molecules system of the conjugate structure also influences the PA intensity, which could increase the molecular conjugation length and could slightly account for the increase of PA intensity. To provide additional confirmation that C1b with the maximum PA intensity can be applied to PDT treatment, ROS yield measurements were also taken and ROS release occurred for all molecules. C1b with the best PA and PT effect was inserted into the liposomal hydrophobic phospholipid bilayer (C1b⊂L) to further investigate its toxicity and cell PA effect.

2. Materials and Methods

Our laboratory has synthesized a series of NIR absorbing molecules, as shown in Figure 1 [26,33]. C was the matrix molecular structure, and its aniline group [40] and long-chain alkyl groups could increase solubility [41] and electron cloud density. C-XY’s series were obtained by applying click reagents, such as TCNQ and F₄-TCNQ. X and Y were the distinct groups shown in Figure 1. The spectral properties of the material are changed by the introduction of click reagents, and the click chemistry modification decreased the separation difficulties of the synthesized C-XY molecules [33].

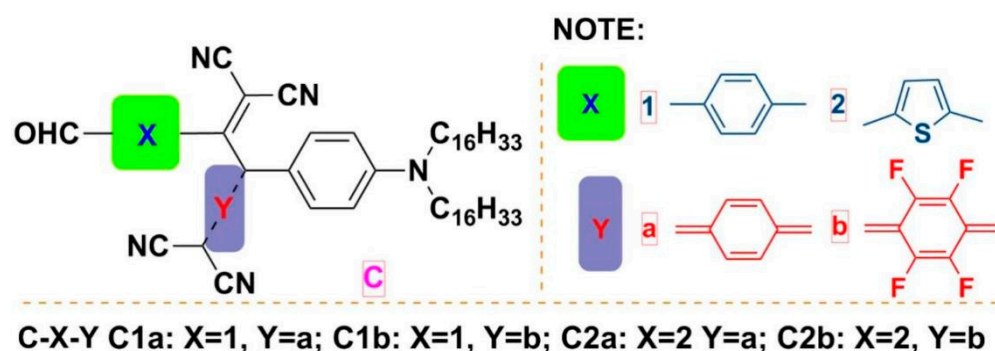


Figure 1. Molecular structures of compounds were named as CXY, X and Y were different modified moieties.

PA imaging in phantom: The C-XY solution was poured into agarose tubes at a 3×10^{-5} mol/L concentration. The model was scanned by using Multispectral Optoacoustic Tomography (MOST) 128 in the wavelength range of 680 to 980 nm. PA intensity was acquired by averaging the pixel intensities of the same regions in images of the same laser intensity.

The heating/cooling curves of C-XY: The 150 μL C-XY solution at a consistency of 3×10^{-5} mol/L in Tetrahydrofuran (THF) were filled into the lid of centrifuge tube which was irradiated with 400 mW power laser sapphire femtosecond laser and a 4 mm diameter mask. The wavelengths were 692 nm for C1a, 842 nm for C1b, 695 nm for C2a, and 866 nm for C2b. The temperatures were recorded by portable infrared thermometer.

The determination of quantum yield of singlet oxygen of C-XY solution: The C-XY molecule and the tetraphenylporphyrin (TPP) used as a reference were each soluble in THF at 3×10^{-5} mol/L concentration. This solution (500 μL) was then incorporated into the centrifuge tube. After that, a pre-made solution of 1,3-diphenylisobenzofuran (DPBF) dissolved in THF at the concentration of 3×10^{-5} mol/L (500 μL) was incorporated in a centrifuge tube. The absorbance of mixtures was determined at 410 nm using a JASCO V-570 spectrometer at intervals of 0, 10, 20, 30, 40, 50, 60, 70, 80, 90, 100 and 110 s after 650 nm laser irradiation with a laser energy density of 4.0 mW/cm².

The preparation of C1b \subset L: L- α -phosphatidylcholine and cholesterol in the weight ratio of 4:1 were solubilized in ethanol solution. C1b solution was then added to the mentioned mixture. The obtained mixture was placed in phosphate-buffered saline (PBS) and stirred for 3 min with an ultrasonic cell disruptor, which enabled the molecules to be embedded in the liposomal hydrophobic phospholipid bilayer.

Cell imaging in agar-based phantom: MCF-7 cells grown in DMEM comprising 10% FBS and 1% penicillin-streptomycin were cultured for 2 h with 10 μM C1b \subset L at 37 $^{\circ}\text{C}$ and 5% CO₂. The cells were subsequently washed three times by cold PBS, which was harvested with trypsin. Approximately 8 million cells from PBS were blended with 1% ultrapure agarose in PBS in a 1:1 ratio and they were syringed into the pores of an agarose gel phantom. Later, the pores were capped with another warm layer of agarose in a 1:1 ratio of agar powder to ultrapure water. After that, the agarose gel phantom described above were cooled at ambient temperature. By using MOST 128, PA imaging was gained at wavelengths from 680 to 980 nm.

3. Discussion and Results

C1b and C2b showed good PA effects were observed as shown in Figure 2a. To obtain further insight into the PA intensity of the molecules, the extinction coefficient (ϵ) of the molecule was also determined. On the basis of the equation of the photothermal mechanism of the PA effect:

$$q \propto \Gamma \epsilon \eta F, \quad (1)$$

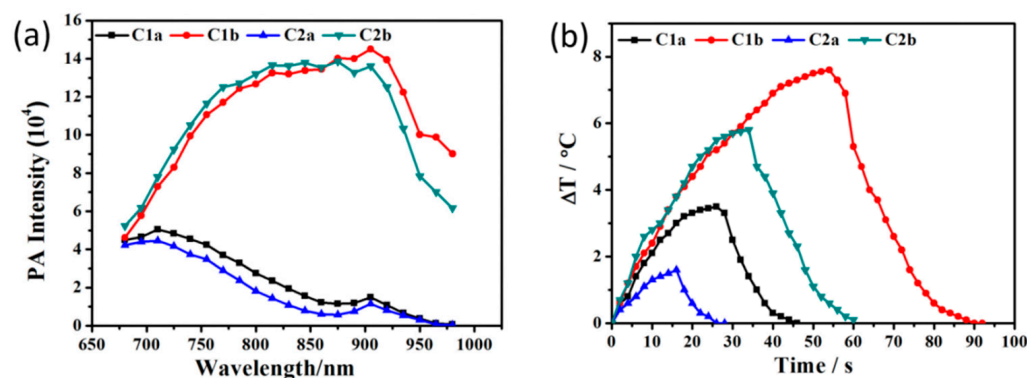


Figure 2. Cont.

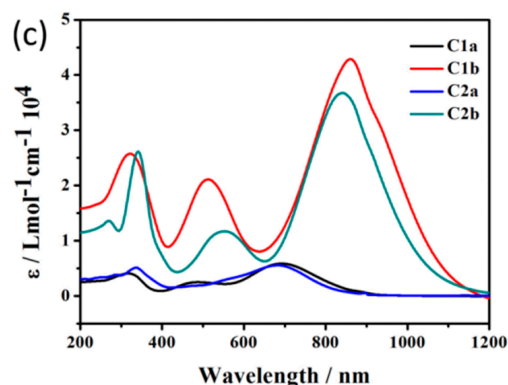


Figure 2. (a) PA intensities of C-XY materials measured for a sample concentration of 3×10^{-5} M in THF. (b) Heating/cooling curves of C-XY as function of time. (c) Molar extinction coefficients (ϵ) of C-XY measured in THF.

The thermal conversion efficiency (η) was also measured from the cooling curves shown in Figure 2b and Figure S2; where Γ shows the Gruneisen parameter (dimensionless), ϵ indicates the optical absorption coefficient (cm^{-1}), η represents the thermal conversion efficiency, as well as F is the local optical fluence ($\text{J}\cdot\text{cm}^{-2}$) [42]. The main parameters contributing to the PA signal are ϵ and η (whose values were measured by fitting the curve to the temperature with time [43]). The UV/Vis/NIR absorption (Figure 2c) were not consistent with the wavelength related PA intensity. (Figure 2a). C1b had the highest ϵ , so that it has the highest PA intensity. The η of the C-XY dyes shown in Table 1 was not consistent with the PA intensity at the same time. The highest η value is for C1a (55.9%), which displayed a low PA intensity. (5.1×10^4), (Table 1). The outcome was not backed up by the equation of the photothermal mechanism of the PA effect. For a range of NIR dyes, the photoacoustic wave may also be associated with the electrostriction of solutions, caused by the transfer of charge from the molecule [44]. The peak PA intensities around 860 nm for both C1b and C2b which were clicked by F_4 -TCNQ. Nevertheless, clicking by TCNQ, both C1a and C2a peak at wavelengths near 690 nm. (Figure 2c). F_4 -TCNQ possessed a strong electron-absorbing group added to F, so its peaks could be shifted to long wavelengths [45]. The PA intensity and η of C1a and C1b which introduced phenyl group were greater than that of C2a and C2b with the introduction of thienyl group. (Table 1).

Table 1. Summary of PA intensity, ϵ , ΔT , τ_s and η of the series of C-XY.

	PA (10^4)	ϵ ($10^4/\text{mol}/\text{cm}$)	ΔT ($^\circ\text{C}$)	τ_s	η (%)
C1a	5.1	0.6	3.5	5.5	55.9
C1b	14.5	4.3	7.6	13.0	38.4
C2a	4.5	0.6	1.6	3.8	39.2
C2b	13.9	3.7	5.8	11.5	33.1

To confirm that C1b which has the highest PA intensity can as well be used as PS, the yield of ROS was investigated (Figure 3 and Figure S4). Based on the previously published method [46], this value (the yield of singlet oxygen of C-XY solution) can be determined by the formula:

$$\Phi_{\Delta}^S = \Phi_{\Delta}^R \frac{K^S F^R}{K^R F^S}, \quad (2)$$

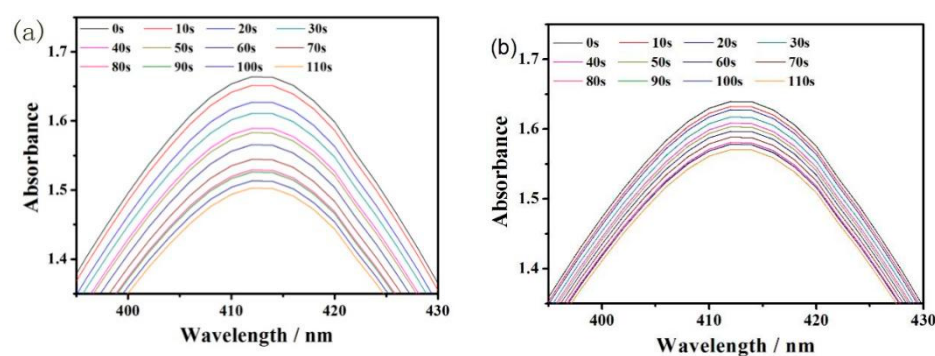


Figure 3. The absorbance values of TPP (a) and C1b (b) THF solution mixed with DPBF after being irradiated 650 nm laser every 10 s.

Among them, the yield of single oxygen ($\Phi = 0.64$) was the reference object. The marked S and R stand for the sample (C-XY) and reference (TPP (5,10,15,20-tetraphenylporphyrin)), separately. K was the linear relationship slope between the absorbance value (ΔOD) of DPBF (1,3-diphenylisobenzofuran) at 410 nm and the time of excitation T (Figure S4). F as an absorption correction factor ($F = 1 - 10^{-OD}$). OD was the absorbance value of the solution at the laser light wavelength [47]. The OD of C1b was 0.24 according to Figure S4 with a K^S of 0.00048. The ROS yield of C1b was 24.0%, which indicates the potential use of C1b for PDT treatment.

For the demonstration of further applications of a series of C-XY in PA imaging, C1b was packed in a pre-made bilayer of hydrophobic liposomes, which were extensively used as drug delivery carriers [48,49]. L- α -phosphatidylcholine and cholesterol in the weight ratio of 4:1 were solubilized in ethanol solution. Subsequently, the THF solution of C1b was incorporated to the premixed ethanol solution as described above. The obtained solution was added to phosphate-buffered saline (PBS) and agitated continuously for 1 hour. C1b molecules were perfectly inserted into the liposomal hydrophobic phospholipid bilayer by hydrophobic interaction [50]. The morphology of C1b \subset L in phosphate-buffered saline was studied using transmission electron microscopy (TEM). When the mass ratio of C1b to phospholipid was 1:10, the vesicles of C1b \subset L had a uniform structure with a dimension of 53 ± 50 nm (Figure 4a). The hydrodynamic diameter of C1b \subset L was determined using dynamic light scattering (DLS) technique with a narrow size distribution of 64 ± 17 nm (Figure S5). The C1b \subset L with a mass ratio of 1:10 showed high absorption at 860 nm, which indicated that C1b was succeeded to be mounted in the liposome (Figure 4a). In addition, we also investigated the stability of C1b mixtures and C1b \subset L in the PBS solution. After irradiation at 860 nm at 15 min intervals for 3 h, the absorption of C1b \subset L PBS solution and C1b mixed solution were still higher than 94% (Figure 4b). The absorption of C1b \subset L and C1b solutions remained above 92% after 7 days (Figure 4c), and the heating/cooling curves of C1b \subset L and C1b remained nearly constant over three consecutive times (Figure 4d). On the basis of Figure 4b–d, C1b \subset L and C1b have excellent stability under both chemical and physical conditions.

Human breast cancer MCF-7 cells were used as a model cell line and the C1b \subset L served as a control agent for PA imaging *in vitro*. The MCF-7 cells ($\sim 10^7$ cells) grown on culture dishes with C1b \subset L (10 mM based on C1b molecule) were incubated at 37 °C for 2 h. The treated cells in PBS and 1% ultra-pure agarose solution were mixed at a volume ratio of 1:1 and then incorporated into the holes of the pre-made agarose gel model. PA imaging was determined with MSOT 128 under 690 nm laser excitation. PA imaging was performed by recording the PA signal of C1b \subset L in the cells in the agarose gel. Since the ratio of C1b embedded in liposomes and C1b \subset L that was loaded into MCF-7 cells was not 100%, the PA intensity of C1b \subset L in cells could still achieve 1.3×10^4 (Figure 5). The cellular toxicity of C1b \subset L nanoparticles was assessed by CCK-8 assay to ascertain the metabolic viability of MCF-7 cells [51]. Under our experimental conditions, there was no significant cytotoxicity detected at concentrations up to 10 mM (Figure S6).

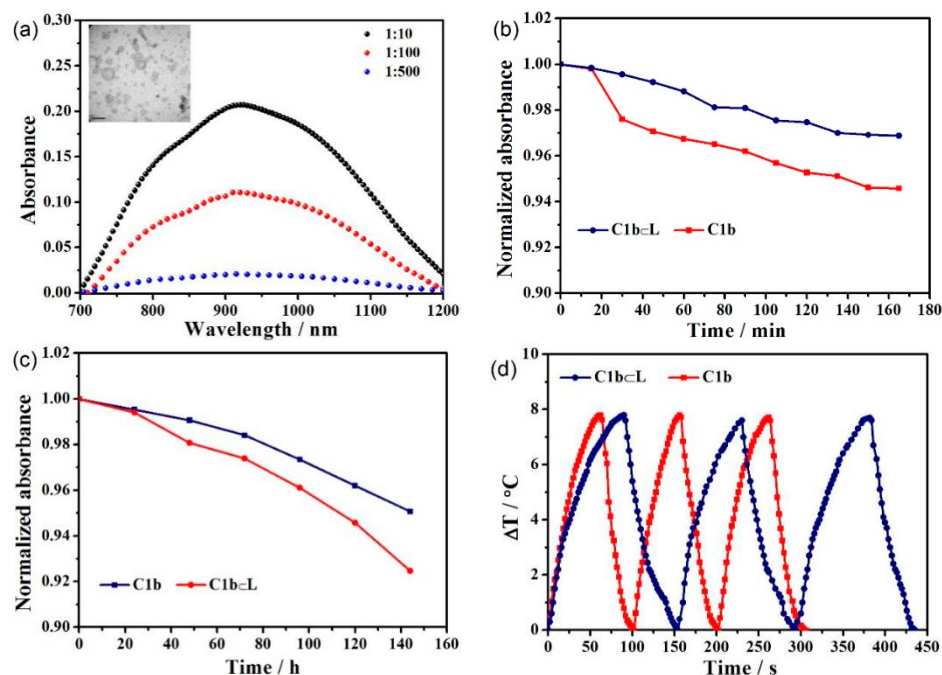


Figure 4. (a) UV/Vis/NIR absorption spectra of C1b⊂L with different ratios of C1b to liposomes in PBS and TEM images of C1b⊂L. (b) The UV/Vis/NIR absorption spectra were estimated after the solution of C1b and C1b⊂L illuminating in every 15 min at 860 nm. (c) The UV/Vis/NIR absorption spectra were estimated after the solution of C1b and C1b⊂L placing 24 h at 860 nm. (d) Thermal conversion efficiency of the solution of C1b and C1b⊂L was measured for continuous 3 times.

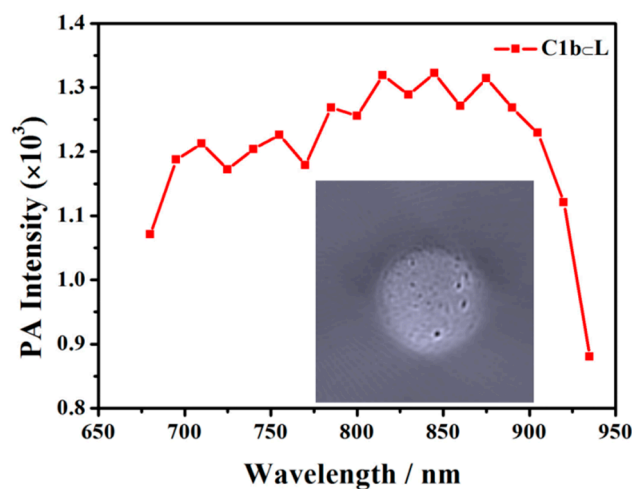


Figure 5. PA imaging of C1b⊂L incubated in cells and the photo of agarose gel phantom loaded with C1b⊂L incubated in cells.

4. Conclusions

In summary, a series of organic molecules with PA and PT effects were characterized with click TCNQ, F₄-TCNQ, respectively. NIR dyes consisting of phenyl clicks has the higher PA intensities compared to NIR dyes consisting of thiophene clicks, and the introduction of the click reagent F₄-TCNQ leads to peaks of PA intensity that are red-shifted. At the same time, C1b with optimal PA effect can generate ROS and perform PDT treatment. In addition, C1b was packed into nano-sized liposomes for further application to cells. It was demonstrated that the PA intensity was high when the liposomes remained in the cells with the molecules for 2 h, while the toxicity of the hydrophobic phospholipid bilayer (C1b⊂L)

embedded in the liposomes was low, which suggests that organic molecules probably have a high potential for the detection as well as treatment of tumors in vivo.

Supplementary Materials: The following are available online <https://www.mdpi.com/article/10.3390/molecules27072329/s1>. Figure S1. (a) UV/Vis/NIR absorption spectra of C1b \subset L with different ratios of C1b to liposomes in PBS and TEM images of C1b \subset L. (b) The UV/Vis/NIR absorption spectra were estimated after the solution of C1b and C1b \subset L illuminating in every 15 min at 860 nm. (c) The UV/Vis/NIR absorption spectra were estimated after the solution of C1b and C1b \subset L placing 24 h at 860 nm. Figure S2. Time constants for heat transfer of C-XY were acquired by applying the linear time data from cooling period. Figure S3. C1a, C1b, C2a, C2b, TPP in THF with DPBF for 10 s at a time under a 650 nm light. Figure S4. Linear fit of time and Δ OD at UV absorption of 410 nm. Figure S5. (a) UV absorption spectra of different ratios of phospholipid-coated C1b (C1b \subset L) and transmission electron micrographs of the inclusions (b) Particle size test distribution of C1b \subset L. Figure S6. MCF-7 cell viability incubated with C1b \subset L measured by the CCK-8 assay. Results are presented as the mean \pm SD in triplicate.

Author Contributions: Conceptualization, D.W.; methodology, D.W.; validation, L.W.; resources, Z.M.; writing—original draft, Z.M.; writing—original draft, W.Z.; Data curation, Y.C.; investigation, L.L.; writing—review & editing, L.W.; writing—review & editing, D.W. All authors have read and agreed to the published version of the manuscript.

Funding: This work was supported by the National Natural Science Foundation of China (No. 52173263), the Natural Science Foundation of Anhui Province, China (No. 2108085J11), the Regional Innovation Capability Guidance Program of Shaanxi (No. 2022QFY03-02).

Institutional Review Board Statement: Not applicable.

Informed Consent Statement: Not applicable.

Data Availability Statement: Not applicable.

Acknowledgments: The authors thank the reviewers for their critical reading of the manuscript.

Conflicts of Interest: The authors declare no conflict of interest.

Sample Availability: Not applicable.

References

1. Dragulescu-Andrasi, A.; Kothapalli, S.-R.; Tikhomirov, G.A.; Rao, J.H.; Gambhir, S.S. Activatable Oligomerizable Imaging Agents for Photoacoustic Imaging of Furin-Like Activity in Living Subjects. *J. Am. Chem. Soc.* **2013**, *135*, 11015–11022. [[CrossRef](#)] [[PubMed](#)]
2. Attia, A.B.E.; Balasundaram, G.; Moothanchery, M.; Dinish, U.S.; Bi, R.Z.; Ntziachristos, V.; Olivo, M. A review of clinical photoacoustic imaging: Current and future trends. *Photoacoustics* **2019**, *16*, 100144. [[CrossRef](#)]
3. Wang, L.V.; Hu, S. Photoacoustic Tomography: In Vivo Imaging from Organelles to Organs. *Science* **2012**, *335*, 1458–1462. [[CrossRef](#)]
4. Ntziachristos, V.; Razansky, D. Molecular Imaging by Means of Multispectral Optoacoustic Tomography (MSOT). *Chem. Rev.* **2010**, *110*, 2783–2794. [[CrossRef](#)] [[PubMed](#)]
5. Xie, H.H.; Liu, M.Q.; You, B.H.; Luo, G.H.; Chen, Y.; Liu, B.L.; Jiang, Z.Y.; Chu, P.K.; Shao, J.D.; Yu, X.F. Biodegradable Bi₂O₂Se Quantum Dots for Photoacoustic Imaging-Guided Cancer Photothermal Therapy. *Small* **2020**, *16*, e1905208. [[CrossRef](#)]
6. Tian, Y.; Younis, M.R.; Tang, Y.X.; Liao, X.; He, G.; Wang, S.J.; Teng, Z.G.; Huang, P.; Zhang, L.J.; Lu, G.M. Dye-loaded mesoporous polydopamine nanoparticles for multimodal tumor theranostics with enhanced immunogenic cell death. *J. Nanobiotechnol.* **2021**, *19*, 365. [[CrossRef](#)] [[PubMed](#)]
7. Ren, M.S.; Zhou, J.J.; Song, Z.Y.; Mei, H.; Zhou, M.; Fu, Z.F.; Han, H.Y.; Zhao, L. Aptamer and RVG functionalized gold nanorods for targeted photothermal therapy of neurotropic virus infection in the mouse brain. *Chem. Eng. J.* **2021**, *411*, 128557. [[CrossRef](#)]
8. Huang, P.; Lin, J.; Li, W.; Rong, P.; Wang, Z.; Wang, S.; Wang, X.; Sun, X.; Aronova, M.; Niu, G.; et al. Biodegradable Gold Nanovesicles with an Ultrastrong Plasmonic Coupling Effect for Photoacoustic Imaging and Photothermal Therapy. *Angew. Chem. Int. Ed.* **2013**, *52*, 13958–13964. [[CrossRef](#)]
9. Lee, S.-Y.; Shieh, M.-J. Platinum(II) Drug-Loaded Gold Nanoshells for Chemo-Photothermal Therapy in Colorectal Cancer. *ACS Appl. Mater. Interfaces* **2020**, *12*, 4254–4264. [[CrossRef](#)]
10. Homan, K.A.; Souza, M.; Truby, R.; Luke, G.P.; Green, C.; Vreeland, E.; Emelianov, S. Silver Nanoplate Contrast Agents for in Vivo Molecular Photoacoustic Imaging. *ACS Nano* **2012**, *6*, 641–650. [[CrossRef](#)]

11. Huang, C.; Zhang, Z.; Guo, Q.; Zhang, L.; Fan, F.; Qin, Y.; Wang, H.; Zhou, S.; Ou-Yang, W.; Sun, H.; et al. A Dual-Model Imaging Theragnostic System Based on Mesoporous Silica Nanoparticles for Enhanced Cancer Phototherapy. *Adv. Health Mater.* **2019**, *8*, e1900840. [[CrossRef](#)] [[PubMed](#)]
12. Fan, Q.L.; Cheng, K.; Yang, Z.; Zhang, R.P.; Yang, M.; Hu, X.; Ma, X.W.; Bu, L.H.; Lu, X.M.; Xiong, X.X.; et al. Perylene-Diimide-Based Nanoparticles as Highly Efficient Photoacoustic Agents for Deep Brain Tumor Imaging in Living Mice. *Adv. Mater.* **2015**, *27*, 843–847. [[CrossRef](#)] [[PubMed](#)]
13. Cao, J.; Chi, J.N.; Xia, J.F.; Zhang, Y.R.; Han, S.C.; Sun, Y. Iodinated Cyanine Dyes for Fast Near-Infrared-Guided Deep Tissue Synergistic Phototherapy. *ACS Appl. Mater. Interfaces* **2019**, *11*, 25720–25729. [[CrossRef](#)] [[PubMed](#)]
14. Rabiee, N.; Yaraki, M.T.; Garakani, S.M.; Ahmadi, S.; Lajevardi, A.; Bagherzadeh, M.; Rabiee, M.; Tayebi, L.; Tahriri, M.; Hamblin, M.R. Recent advances in porphyrin-based nanocomposites for effective targeted imaging and therapy. *Biomaterials* **2020**, *232*, 119707. [[CrossRef](#)]
15. Zhen, X.; Pu, K.; Jiang, X. Photoacoustic Imaging and Photothermal Therapy of Semiconducting Polymer Nanoparticles: Signal Amplification and Second Near-Infrared Construction. *Small* **2021**, *17*, e2004723. [[CrossRef](#)]
16. Ntziachristos, V. Going deeper than microscopy: The optical imaging frontier in biology. *Nat. Methods* **2010**, *7*, 603–614. [[CrossRef](#)]
17. Liang, P.X.; Li, Z.Q.; Mi, Y.S.; Yang, Z.; Wang, D.; Cao, H.; He, W.; Yang, H. Pyrene-Based Small Molecular Nonlinear Optical Materials Modified by “Click-Reaction”. *J. Electron. Mater.* **2015**, *44*, 2883–2889. [[CrossRef](#)]
18. Wang, D.; Guo, Q.S.; Gao, H.; Yang, Z.; Xing, Y.; Cao, H.; He, W.L.; Wang, H.H.; Gu, J.M.; Hu, H.Y. The application of double click to synthesize a third-order nonlinear polymer containing donor-acceptor chromophores. *Polym. Chem.* **2016**, *7*, 3714–3721. [[CrossRef](#)]
19. Liu, X.; Wang, D.; Gao, H.; Yang, Z.; Xing, Y.; Cao, H.; He, W.L.; Wang, H.H.; Gu, J.M.; Hu, H.Y. Nonlinear optical properties of symmetrical and asymmetrical porphyrin derivatives with click chemistry modification. *Dye. Pigment.* **2016**, *134*, 155–163. [[CrossRef](#)]
20. Wang, D.; Zhang, R.R.; Gao, H.; Wang, X.K.; Wang, H.H.; Yang, Z.; He, W.L.; Cao, H.M.; Gu, J.M.; Hu, H.Y.; et al. Energy-level tuning of poly(p-phenylenebutadiynylene) derivatives by click chemistry-type postfunctionalization of side-chain alkynes. *React. Funct. Polym.* **2016**, *105*, 114–121. [[CrossRef](#)]
21. Wang, D.; Han, H.H.; Gao, H.; Yang, Z.; Xing, Y.; Cao, H.; He, W.L.; Wang, H.H.; Gu, J.M.; Hu, H.Y. Synthesis and evaluation of simple molecules for dye sensitized solar cells. *Synth. Met.* **2016**, *220*, 41–47. [[CrossRef](#)]
22. Han, P.B.; Yang, Z.; Cao, H.; He, W.L.; Wang, D.; Zhang, J.J.; Xing, Y.; Gao, H. Nonlinear optical properties of the novel kind of organic donor-acceptor thiophene derivatives with click chemistry modification. *Tetrahedron* **2017**, *73*, 6210–6216. [[CrossRef](#)]
23. Han, P.B.; Wang, D.; Gao, H.; Zhang, J.J.; Xing, Y.; Yang, Z.; Cao, H.; He, W.L. Third-order nonlinear optical properties of cyanine dyes with click chemistry modification. *Dye. Pigment.* **2018**, *149*, 8–15. [[CrossRef](#)]
24. Li, L.L.; Wang, D.; Wang, L.; Ramella, D.; Wang, H.; Gao, H.; Zhang, J.J.; Xing, Y.; Li, B.N.; Yang, Z.; et al. The photoacoustic effect of near-infrared absorbing porphyrin derivatives prepared via click chemistry. *Dye. Pigment.* **2018**, *148*, 501–507. [[CrossRef](#)]
25. Çağatay, D. Polycyclic aromatic hydrocarbon-substituted push-pull chromophores: An investigation of optoelectronic and nonlinear optical properties using experimental and theoretical approaches. *Turk. J. Chem.* **2021**, *45*, 1375–1390. [[CrossRef](#)]
26. Zhang, W.S.; Wang, D.; Cao, H.; Yang, H.I. Energy level tunable pre-click functionalization of [60]fullerene for nonlinear optics. *Tetrahedron* **2014**, *70*, 573–577. [[CrossRef](#)]
27. Rao, P.S.; Brix, S.; Shaikh, D.B.; Al Kobaisi, M.; Lessard, B.H.; Bhosale, S.V.; Bhosale, S.V. The Effect of TCNE and TCNQ Acceptor Units on Triphenylamine-Naphthalenediimide Push-Pull Chromophore Properties. *Eur. J. Org. Chem.* **2021**, *2021*, 2615–2624. [[CrossRef](#)]
28. Rao, P.S.; More, V.G.; Jangale, A.D.; Bhosale, S.V.; Bhosale, R.S.; Puyad, A.L.; Chen, J.Y.; Li, J.L.; Bhosale, S.V.; Gupta, A.; et al. A series of V-shaped small molecule non-fullerene electron acceptors for efficient bulk-heterojunction devices. *Dye. Pigment.* **2019**, *171*, 107677. [[CrossRef](#)]
29. Tian, S.; Cao, H.; Yang, Z.; Zhao, Y.; He, W.; Gao, H. Synthesis of pyrene-based materials with third-order nonlinearity optical property by click chemistry modification. *Pigment Resin Technol.* **2021**; ahead-of-print. [[CrossRef](#)]
30. Banziger, S.D.; Clendening, R.A.; Oxley, B.M.; Ren, T. Spectroelectrochemical and Computational Analysis of a Series of Cycloaddition-Retroelectrocyclization-Derived Donor-Acceptor Chromophores. *J. Phys. Chem. B* **2020**, *124*, 11901–11909. [[CrossRef](#)]
31. Raheem, A.A.; Kumar, C.; Shanmugam, R.; Murugan, P.; Praveen, C. Molecular engineering of twisted dipolar chromophores for efficiency boosted BHJ solar cells. *J. Mater. Chem. C* **2021**, *9*, 4562–4575. [[CrossRef](#)]
32. Michinobu, T. Development of N-Type Semiconducting Polymers for Transistor Applications. *J. Photopolym. Sci. Technol.* **2019**, *32*, 563–570. [[CrossRef](#)]
33. Liu, X.; Wang, D.; Gao, H.; Yang, Z.; Xing, Y.; Cao, H.; He, W.; Wang, H.; Gu, J.; Hu, H. Click chemistry functionalization improving the wideband optical-limiting performance of fullerene derivatives. *Phys. Chem. Chem. Phys.* **2016**, *18*, 7341–7348. [[CrossRef](#)]
34. Rout, Y.; Mobin, S.M.; Misra, R.; Rout, Y. Tetracyanobutadiene (TCBD) functionalized benzothiadiazole derivatives: Effect of donor strength on the [2+2] cycloaddition-retroelectrocyclization reaction. *New J. Chem.* **2019**, *43*, 12299–12307. [[CrossRef](#)]
35. Cheng, S.; Li, K.; Hu, J.; He, J.; Zeller, M.; Xu, Z. Building Conjugated Donor-Acceptor Cross-Links into Metal-Organic Frameworks for Photo- and Electroactivity. *ACS Appl. Mater. Interfaces* **2020**, *12*, 19201–19209. [[CrossRef](#)]

36. Sharma, R.; Thomas, M.B.; Misra, R.; D'Souza, F. Strong Ground- and Excited-State Charge Transfer in C₃-Symmetric Truxene-Derived Phenothiazine-Tetracyanobutadine and Expanded Conjugates. *Angew. Chem. Int. Ed.* **2019**, *58*, 4350–4355. [[CrossRef](#)] [[PubMed](#)]
37. Mi, Y.S.; Liang, P.X.; Yang, Z.; Wang, D.; He, W.L.; Cao, H.; Yang, H. Synthesis and co-assembly of gold nanoparticles functionalized by a pyrene-thiol derivative. *RSC Adv.* **2015**, *5*, 140–145. [[CrossRef](#)]
38. Wang, D.; Guo, Q.S.; Gao, H.; Yang, Z.; Cao, H.; He, W.L.; Wang, H.H. Facile synthesis of functional poly(vinylene sulfide)s containing donor-acceptor chromophores by a double click reaction. *RSC Adv.* **2016**, *6*, 59327–59332. [[CrossRef](#)]
39. Liu, W.Y.; Li, B.N.; Gao, H.; Wang, D.; Wang, L.; Yang, Z.; Cao, H.; He, W.L.; Wang, H.; Zhang, J.J.; et al. NIR absorbing thiophene derivatives with photoacoustic and photothermal effect used in drug release. *Dye. Pigment.* **2018**, *162*, 331–338. [[CrossRef](#)]
40. Ramnivasirtha, P.; Balaji, J.; Sneha, X.C.M.; Karthik, P.S.; Gajalaskhmi, D.; Vinitha, G. Studies on growth, optical, dielectric, and third-order nonlinearity of 4-methyl N-(4-chlorobenzylidene)aniline (4CBT) crystal. *J. Mater. Sci. Mater. Electron.* **2020**, *31*, 18234–18247. [[CrossRef](#)]
41. Tsuda, Y.; Kojima, M.; Matsuda, T.; Oh, J.M. Soluble Polyimides Based on Long-chain Alkyl Groups via Amide Linkages. *Polym. J.* **2008**, *40*, 354–366. [[CrossRef](#)]
42. Ahn, H.-Y.; Yao, S.; Wang, X.; Belfield, K.D. Near-Infrared-Emitting Squaraine Dyes with High 2PA Cross-Sections for Multiphoton Fluorescence Imaging. *ACS Appl. Mater. Interfaces* **2012**, *4*, 2847–2854. [[CrossRef](#)] [[PubMed](#)]
43. Huynh, E.; Jin, C.S.; Wilson, B.C.; Zheng, G. Aggregate Enhanced Trimodal Porphyrin Shell Microbubbles for Ultrasound, Photoacoustic, and Fluorescence Imaging. *Bioconjug. Chem.* **2014**, *25*, 796–801. [[CrossRef](#)] [[PubMed](#)]
44. Xu, M.; Wang, L.V. Photoacoustic imaging in biomedicine. *Rev. Sci. Instrum.* **2006**, *77*, 41101. [[CrossRef](#)]
45. Braun, S.; Salaneck, W.R. Fermi level pinning at interfaces with tetrafluorotetracyanoquinodimethane (F4-TCNQ): The role of integer charge transfer states. *Chem. Phys. Lett.* **2007**, *438*, 259–262. [[CrossRef](#)]
46. Thomas, A.P.; Babu, P.S.S.; Nair, S.A.; Ramakrishnan, S.; Ramaiah, D.; Chandrashekar, T.K.; Srinivasan, A.; Pillai, M.R. meso-Tetrakis(p-sulfonatophenyl)N-Confused Porphyrin Tetrasodium Salt: A Potential Sensitizer for Photodynamic Therapy. *J. Med. Chem.* **2012**, *55*, 5110–5120. [[CrossRef](#)]
47. An, H.-W.; Qiao, S.-L.; Hou, C.-Y.; Lin, Y.-X.; Li, L.-L.; Xie, H.-Y.; Wang, Y.; Wang, L.; Wang, H. Self-assembled NIR nanovesicles for long-term photoacoustic imaging in vivo. *Chem. Commun.* **2015**, *51*, 13488–13491. [[CrossRef](#)] [[PubMed](#)]
48. Li, W.; Wang, L.; Zhang, J.-P.; Wang, H. Bis-pyrene-based supramolecular aggregates with reversibly mechanochromic and vapochromic responsiveness. *J. Mater. Chem. C* **2014**, *2*, 1887–1892. [[CrossRef](#)]
49. Eisele, D.M.; Knoester, J.; Kirstein, S.; Rabe, J.P.; Bout, D.A.V. Uniform exciton fluorescence from individual molecular nanotubes immobilized on solid substrates. *Nat. Nanotechnol.* **2009**, *4*, 658–663. [[CrossRef](#)]
50. Yao, H.; Kagoshima, Y.; Kitamura, S.-I.; Isohashi, T.; Ozawa, A.Y.; Kimura, K. Superstructures of Mesoscopic Monomolecular Sheets of Thiocyanine J Aggregates in Solution. *Langmuir* **2003**, *19*, 8882–8887. [[CrossRef](#)]
51. Barni, E.; Savarino, P.; Pelizzetti, E.; Rothenberger, G. Synthesis, Surface Activity and Micelle Formation of Novel Cyanine Dyes. *Helv. Chim. Acta* **1981**, *64*, 1943–1948. [[CrossRef](#)]